

Frequency-Aware Gaussian Splatting Decomposition

Yishai Lavi Leo Segre Shai Avidan

Tel Aviv University

https://yishailavi.github.io/nerfstudio_lap

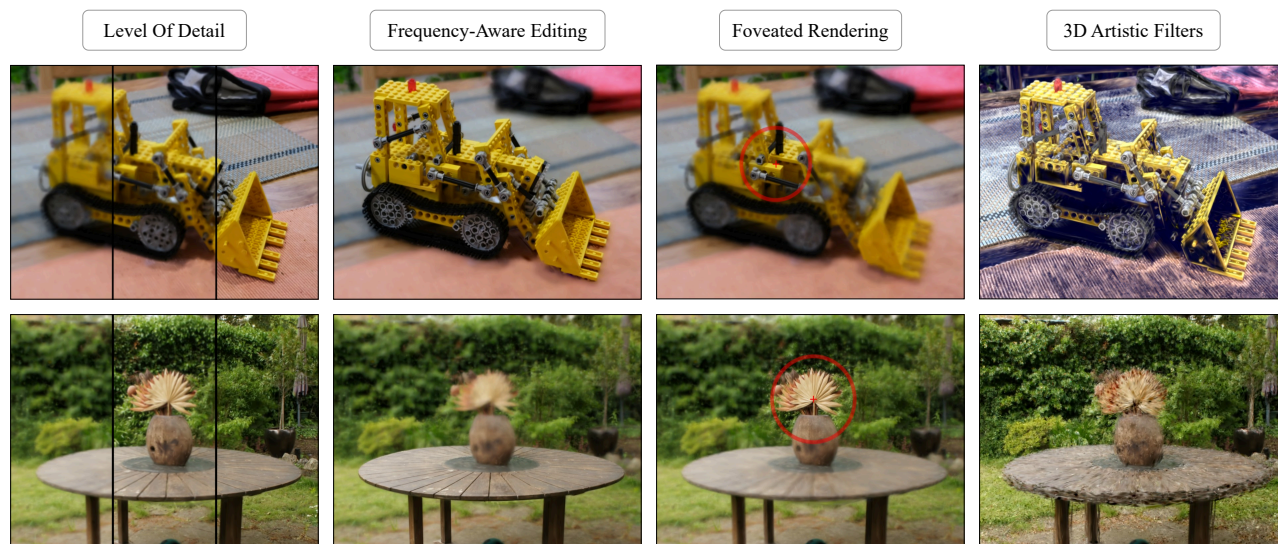


Figure 1. **Frequency-Aware Decomposition for 3D Gaussian Splatting:** We introduce a frequency-aware decomposition for 3D Gaussian Splatting (3D-GS). The decomposition assigns different Gaussians to different levels of the Laplacian Pyramid of the input images. This enables Level of Detail (LOD) rendering, Frequency-aware 3D editing, Foveated rendering, and 3D artistic filters.

Abstract

3D Gaussian Splatting (3D-GS) has revolutionized novel view synthesis with its efficient, explicit representation. However, it lacks frequency interpretability, making it difficult to separate low-frequency structures from fine details. We introduce a frequency-decomposed 3D-GS framework that groups 3D Gaussians that correspond to subbands in the Laplacian Pyramids of the input images.

Our approach enforces coherence within each subband (i.e., group of 3D Gaussians) through dedicated regularization, ensuring well-separated frequency components. We extend color values to both positive and negative ranges, allowing higher-frequency layers to add or subtract residual details. To stabilize optimization, we employ a progressive training scheme that refines details in a coarse-to-fine manner.

Beyond interpretability, this frequency-aware design un-

locks a range of practical benefits. Explicit frequency separation enables advanced 3D editing and stylization, allowing precise manipulation of specific frequency bands. It also supports dynamic level-of-detail control for progressive rendering, streaming, foveated rendering and fast geometry interaction. Through extensive experiments, we demonstrate that our method provides improved control and flexibility for emerging applications in scene editing and interactive rendering. Our code will be made publicly available.

1. Introduction

Novel view synthesis has undergone a remarkable evolution in recent years, propelled by the success of neural representation and optimization. First, Neural Radiance Fields (NeRFs) [10] and later 3D Gaussian Splatting (3D-GS) [5] have enabled the creation of high-fidelity scene reconstruc-

tions and photorealistic renderings from sparse input views.

Adding multi-resolution capabilities to 3D-GS representation can greatly help in tasks such as anti-aliasing, Level-Of-Details, or streaming, and considerable amount of work was done in this direction. Here, we take this idea one step further and merge 3D-GS with Laplacian Pyramids of images.

Specifically, we propose to group Gaussians based on the frequency sub-bands of the Laplacian pyramid of the input images. This allows us to create a structured hierarchy within 3D-GS, where each group of 3D Gaussians is used to render a specific sub-band across all input images. This design enables us to selectively render low-pass or high-pass components at will, offering a controllable frequency decomposition analogous to classical 2D image pyramids, but directly in 3D. Rendering only the first k sub-bands yields a low-frequency rendering of the scene, while including all sub-bands produces a high-fidelity, full-frequency representation comparable to standard 3D-GS.

Beyond the fundamental advantage of greater interpretability, our frequency-aware 3D-GS representation opens the door to novel applications. Similar to level-of-detail systems, it naturally supports progressive rendering and streaming, allowing incremental refinement of a scene. Furthermore, it facilitates foveated rendering (rendering high-frequency detail only in a region of interest), frequency-aware 3D editing, scene stylization via consistent artistic filters that manipulate specific frequency ranges, and faster interaction with the scene’s geometry. We demonstrate that these enhancements go beyond simple scene reconstruction, highlighting the broad utility of a frequency-decomposed 3D Gaussian Splatting framework for both research and practical deployment. Fig. 1 demonstrates some of the mentioned applications.

In summary, our main contribution is a **frequency-aware 3D Gaussian splatting decomposition**, that enables explicit control over scene details across different frequency levels. This decomposition facilitates various applications, including progressive rendering, streaming, foveated rendering, geometry interaction, and advanced 3D editing.

2. Related Work

2.1. Novel View Synthesis

Novel view synthesis aims to generate photorealistic images of a scene from previously unseen viewpoints, typically using only a sparse set of reference images as input. Early approaches in this field often relied on explicit scene geometry, such as depth-based image warping [13], to synthesize novel views. More recently, Neural Radiance Fields (NeRF) [10] have revolutionized the field by representing a 3D scene as a continuous function, parameterized by a multi-layer perceptron (MLP), that predicts color and

density at any 3D coordinate and viewing direction. This enables high-quality view synthesis by querying the scene using volume rendering. However, despite their success, NeRF-based methods are computationally expensive, making both training and real-time rendering challenging. To address these limitations, a more recent approach, 3D Gaussian Splatting (3D-GS) [5], represents the scene as a set of explicit, oriented Gaussian primitives and employs a fast differentiable rasterizer to render novel views. This technique significantly reduces computational overhead while maintaining high-quality rendering results.

2.2. Frequency-Aware Representations

Many computer vision and graphics algorithms leverage frequency decomposition techniques to process and analyze images effectively. Classical methods such as the Laplacian pyramid [3] enable multi-scale image representations, facilitating detail manipulation and compression. The Image Fourier transform decomposes signals into frequency components, widely used in filtering and texture analysis, while wavelet transforms [7] provide localized frequency representations useful for image denoising and compression. Inspired by these techniques, recent neural representations incorporate frequency awareness to improve learning and reconstruction quality. [18] introduce Polynomial Neural Fields (PNFs) and demonstrate frequency-based manipulation of neural fields using Fourier PNFs. [21] propose progressive frequency training to accelerate the training and rendering of neural radiance fields.

Similarly to our approach, [20] utilize a Fourier-based loss, but apply it to guide Gaussian densification in a coarse-to-fine manner to mitigate over-reconstruction. In contrast, we use it to group Gaussians into distinct frequency sub-bands of the scene.

2.3. Level of Detail in 3D Gaussian Splatting

Similar to classical computer vision techniques, some 3D Gaussian Splatting (3D-GS) methods incorporate level-of-detail representations for various tasks. [17] introduce multi-scale Gaussians to improve anti-aliasing and enhance rendering efficiency at lower resolutions. [12] propose an octree-based data structure [8] to hierarchically organize Gaussians with anchors, ensuring consistent rendering speed across different resolutions and scales, particularly in large scenes. However, while these methods incorporate level-of-detail mechanisms, they lack explicit frequency-based regularization as in our approach, leading to missing structural information rather than just coarser details at lower levels of detail.

3. Method

Our method is based on the foundational framework of 3D Gaussian splatting [5]. By extending this method, we intro-

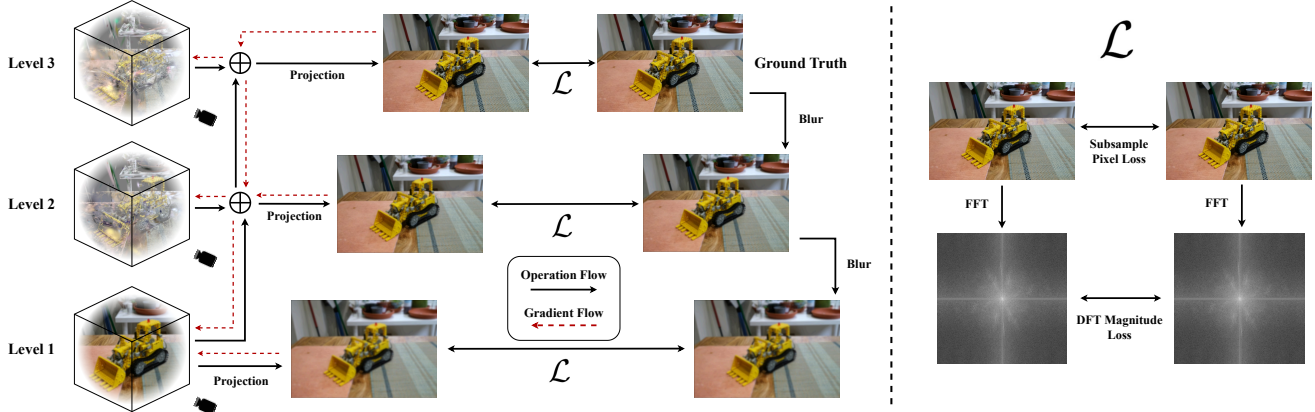


Figure 2. **Architecture Overview:** (Left) We group 3D Gaussians based on their contribution to different frequency levels and progressively accumulate them to construct a multi-scale representation. The accumulated contribution of the first k Gaussian groups is designed to match a corresponding low-pass filtered version of the ground truth image, ensuring that each individual level aligns with the associated band in the Laplacian pyramid of the input images. (Middle) The training pipeline enforces this frequency-aware decomposition by supervising projections at different levels against progressively blurred ground truth images. (Right) We incorporate a frequency-domain loss, combining pixel-wise supervision with Discrete Fourier Transform (DFT) magnitude regularization to ensure that each frequency level contributes meaningfully to the final rendered image, preserving structural integrity while capturing high-frequency details.

duce a mechanism to group Gaussians based on their contribution to different frequency bands of the images. These groups, referred to as "levels", enable a hierarchical representation akin to the Image Laplacian Pyramid [3] in classical computer vision. Each frequency level captures progressively finer details, from diffuse colors and general structure to high-frequency variations, optimizing both the rendering process and frequency-aware modeling.

To render a scene at a chosen frequency level, all Gaussians up to that frequency level are rendered in a single render pass. In particular, rendering the full-resolution image requires simply rendering all Gaussians in one pass, just as in standard 3D Gaussian splatting.

3.1. Preliminary: 3D Gaussian Splatting

3D Gaussian Splatting (3D-GS) [5] represents a scene as a collection of anisotropic 3D Gaussians $\{G_i\}_{i=1}^N$, providing a structured, explicit alternative to neural-based representations.

The initialization of 3D-GS typically starts from a point cloud $\{x_i\}_{i=1}^N$ obtained via Structure-from-Motion (SfM). Each point x_i in this cloud is assigned a 3D Gaussian representation G_i , which is defined by a mean position μ_i and a covariance matrix Σ_i . The covariance is decomposed as:

$$\Sigma_i = \mathcal{R} \mathcal{S} \mathcal{S}^T \mathcal{R}^T, \quad (1)$$

where \mathcal{S} represents a scaling matrix controlling the extent of the Gaussian, and \mathcal{R} is a rotation matrix ensuring Σ_i remains positive semi-definite. Additionally, each Gaussian stores appearance information through spherical harmonics

and an opacity value α_i , which contributes to the blending process.

Rendering in 3D-GS involves projecting the 3D Gaussians into 2D space, converting them into 2D Gaussians G'_i . A differentiable rasterization process sorts these 2D Gaussians by depth and blends them according to their opacity. The final color $C(x)$ at a pixel position x is computed as:

$$C(x) = \sum_{j \in M} c_j \sigma_j \prod_{k=1}^{j-1} (1 - \sigma_k), \quad (2)$$

where $\sigma_j = \alpha_j G'_j(x)$, M represents the ordered set of Gaussians contributing to x , and c_j denotes the corresponding color. This differentiable rendering pipeline enables joint optimization of all Gaussian attributes during training, facilitating high-quality view synthesis.

3.2. Gaussian Level Grouping

Fig. 2 gives an overview of our method. We progressively group 3D Gaussians based on their frequency contribution, ensuring that the accumulated rendering of the first k groups matches a corresponding low-pass filtered version of the input. This guarantees that each individual level aligns with the respective frequency band in the Laplacian pyramid of the input images. To enforce frequency-aware consistency, we introduce a dedicated frequency regularization term in the loss function.

To hierarchically represent the scene by frequency levels, our method divides the Gaussians into groups, where each group corresponds to a specific band of frequencies.

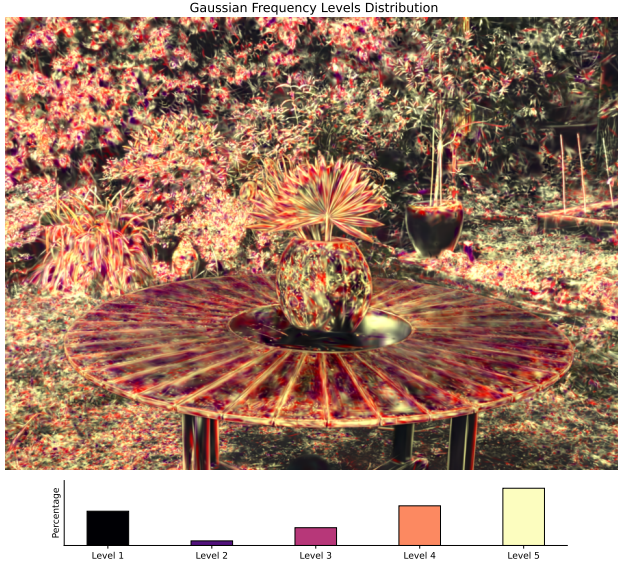


Figure 3. Visualization of the Gaussian frequency levels distribution in the scene. The colormap represents different frequency levels, where lower levels correspond to coarse scene structures and higher levels capture finer details.

The scene is constructed progressively, starting from low frequencies and incorporating higher frequencies over time by adding additional groups. In practice, we modulate each Gaussian G_i with an integer, non-learnable parameter l_i , termed "level", which denotes the frequency group to which the Gaussian belongs. We initialize and update this parameter as follows:

Initialization: Gaussians of the first level are initialized using a Structure-from-Motion (SfM) point cloud, as in the original 3D Gaussian Splatting paper. All Gaussians are assigned an initial level of 1, representing the base frequency group.

Adaptive density control: During training, Gaussians can be split or cloned using the adaptive density control technique from the original method. The newly created Gaussians inherit the same level as their parent.

Progressive Level Introduction: Every K training steps, we introduce a new level to the scene by duplicating all Gaussians in the scene, and assigning the next frequency level to the duplicated Gaussians.

Fig. 3 shows the decomposition of 3D Gaussians to different groups that correspond to different levels of the Laplacian pyramid. As can be seen, the base level requires a considerable amount of Gaussians, while the intermediate low levels require far less, except for the last two levels, that correspond to high frequencies.

3.3. Residual Color Gaussians

Traditional Gaussian Splatting techniques rely on the accumulation of Gaussian colors to render scenes. However,

in our method, higher-level Gaussians contribute details to lower-level Gaussians, such as textures and edges, which cannot be achieved efficiently by simply "adding color". To address this limitation, we introduce Residual Color Gaussians, allowing for both positive and negative color values. This approach compensates for lower-level contributions and facilitates the addition of high-frequency details, achieving a more accurate and detailed hierarchical representation.

Level 1 Gaussians retain colors in the range $[0, 1]$, consistent with the original 3D-GS paper, by using view-dependent spherical harmonic color generation; Given Gaussian G_i and viewing direction d , the rendered color of the Gaussian is calculated by:

$$C_i = SH(G_i, d) \quad (3)$$

Inspired by the Laplacian pyramid [3] in image processing, where residual levels can take both positive and negative values to represent higher-frequency sub-bands, we multiply the color range of all Gaussians at higher levels by 2 and shift down by 1, resulting in a range of $[-1, 1]$:

$$C_i = (SH(G_i, d) \cdot 2) - 1 \quad (4)$$

This simple adjustment is applied before alpha blending and enables subtraction of colors between positive and negative colored Gaussians. The final rendered color is clamped to the range $[0, 1]$. This approach effectively captures high-frequency details, analogously to the functionality of residual levels in the Laplacian pyramid.

3.4. Progressive Rendering of Frequency Bands

As stated above, at inference time, one can render all Gaussians in the scene at once to get the full resolution rendered image. Recall, in the Laplacian Pyramid, one can reconstruct a Gaussian Pyramid by up-sampling and adding each Laplacian level with its successor, resulting in images with progressively finer details. Similarly, to regulate the different frequency levels in our method during the training stage, we render each level of the Gaussian Pyramid separately by combining all Gaussian groups up to the corresponding frequency level.

Importantly, all images are rendered at the same (full) resolution. This ensures that we can accurately regulate the frequencies of the Gaussians in each accumulated level without inadvertently removing valid high-frequency details due to subsampling. Subsampling would remove or alias frequency components above the Nyquist limit [14], making it impossible to determine whether Gaussians truly represent low-frequency information or if their details were simply lost during down-sampling. Rendering at full resolution allows us to preserve and regulate the true frequency content of each level accurately.

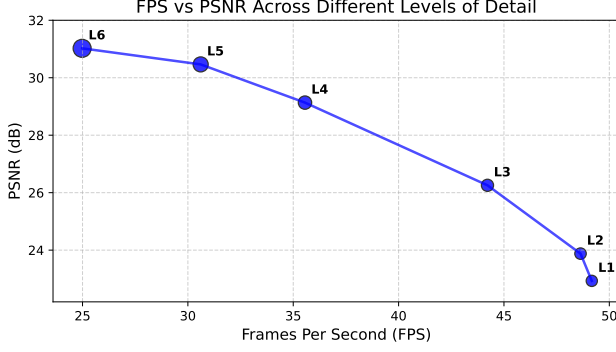


Figure 4. **Progressive Rendering and Streaming:** PSNR as a function of Frames Per Second (FPS), achieved by rendering all levels up to L_k . The model was trained at a resolution of 3115×2078 pixels with six frequency levels, on the kitchen scene from the Mip-NeRF 360 dataset. The marker size radius is proportional to the accumulated number of Gaussians rendered across levels, illustrating the trade-off between fidelity and performance. Rendering more Gaussians increases PSNR but reduces FPS.

Specifically, for a pyramid with L levels, rendering the k 'th frequency level, where $1 \leq k \leq L$, we render all Gaussians G_i that satisfy $l_i \leq k$, results with the following sequence of rendered images:

$$\{\hat{I}_k\}_{k=1}^L, \quad \hat{I}_k \in \mathbb{R}^{H \times W \times 3}, \quad 1 \leq k \leq L \quad (5)$$

3.5. Frequency Regulation and Losses Design

As mentioned earlier, we apply frequency regulation at full resolution. To achieve this, we utilize bilinear interpolation with a scale factor of 0.5 for downsampling, denoted as \downarrow_2 , and bilinear interpolation with a scale factor of 2 for upsampling, denoted as \uparrow_2 .

Hence, given a GT image $I \in \mathbb{R}^{H \times W \times 3}$, in order to regulate the frequency band of the k -th level \hat{I}_k , we construct the low-pass filtered image with:

$$I_k = ((I) \downarrow_2^{L-k}) \uparrow_2^{L-k} \quad (6)$$

This way, we obtain the frequency spectrum of the GT image as it was subsampled $L - k$ times, but we keep it in its original resolution.

To regulate the frequency spectrum, we introduce the frequency magnitude discrepancy term, which helps maintain the desired frequencies in \hat{I}_k . Given an image I_k , let $F_k(u, v)$ denote its Discrete Fourier Transform (DFT) at frequency coordinate (u, v) . Using the frequency magnitudes $|F_k(u, v)|$, we define the frequency magnitude discrepancy term between two images as:

$$d_{\text{DFT}}(I_k, \hat{I}_k) = \frac{1}{UV} \sum_{u=0}^{U-1} \sum_{v=0}^{V-1} \left\| |F_k(u, v)| - |\hat{F}_k(u, v)| \right\| \quad (7)$$

where UV represents the total number of frequency components and $F_k(u, v)$ and $\hat{F}_k(u, v)$ denote the frequency coefficients of images I_k and \hat{I}_k , respectively.

Employing Eq. (7), we will define our frequency magnitude loss by applying the frequency discrepancy term on all levels, except for the last one (as we do not desire to limit its frequency band):

$$\mathcal{L}_{\text{DFT}} = \sum_{k=1}^{L-1} d_{\text{DFT}}(I_k, \hat{I}_k) \quad (8)$$

Furthermore, we adopt a spatial image discrepancy term similar to the one used in the original 3D-GS paper. Specifically, we regulate the k -th frequency level at its corresponding low resolution. To prevent aliasing, we employ the REDUCE operation, as originally introduced in the Laplacian Pyramid framework [3].

Given an image I and a Gaussian kernel \mathcal{G} , the REDUCE operation is defined as a convolution with the kernel followed by subsampling every second row and column:

$$\text{REDUCE}(I) = (I * \mathcal{G})_{::2} \quad (9)$$

To regulate the k -th frequency level, we apply Eq. (9) $L - k$ times to both I_k and \hat{I}_k , yielding:

$$I'_k = \text{REDUCE}^{L-k}(I_k), \quad \hat{I}'_k = \text{REDUCE}^{L-k}(\hat{I}_k) \quad (10)$$

Using the processed images from Eq. (10), we define our spatial image discrepancy term as:

$$d_{\text{IM}}(I_k, \hat{I}_k) = (1 - \lambda_{\text{SSIM}}) |I'_k - \hat{I}'_k| + \lambda_{\text{SSIM}} d_{\text{D-SSIM}}(I'_k, \hat{I}'_k) \quad (11)$$

where d_{IM} combines a pixel-wise difference term with a structural similarity (SSIM) discrepancy, weighted by λ_{SSIM} . Utilizing Eq. (11), the spatial image loss is computed by summing the spatial image discrepancy terms over the rendered and ground truth (GT) levels:

$$\mathcal{L}_{\text{IM}} = \sum_{k=1}^L \lambda_{d_k} d_{\text{IM}}(I_k, \hat{I}_k) \quad (12)$$

Finally, taking Eq. (12) and Eq. (8), our final loss function is defined as:

$$\mathcal{L} = \lambda_{\text{IM}} \mathcal{L}_{\text{IM}} + \lambda_{\text{DFT}} \mathcal{L}_{\text{DFT}} \quad (13)$$

where λ_{IM} and λ_{DFT} are weighting factors balancing the contributions of the spatial and frequency terms, respectively.

4. Results

We evaluate our novel representation by showcasing several applications that are not feasible with the standard 3D-GS implementation, highlighting the versatility and practical advantages of our frequency decomposition beyond conventional reconstruction and view synthesis.

4.1. Datasets

Following the 3D-GS dataset configuration, we evaluated our model across all nine scenes of the Mip-NeRF 360 dataset [1], the Truck and Train scenes from the Tanks & Temples dataset [6], and the Playroom and Dr. Johnson scenes from the Deep Blending dataset [4]. For evaluation, we adopt the same protocol as 3D-GS, selecting every eighth image as part of the test set.

4.2. Implementation details

Our implementation is based on the NerfStudio SplatFacto model [15]. To ensure stable optimization, we begin training with low-resolution images and progressively double the training resolution each time a new frequency level is introduced. A new frequency level is added every $K = 2500$ steps. Upon adding a level, all optimizers and their schedulers are reinitialized, and Gaussian refinement is temporarily disabled for 300 steps. Throughout training, all levels are jointly optimized. Following 3D-GS, we set $\lambda_{SSIM} = 0.2$. Additionally, we empirically set $\lambda_{d_k} = 0.1$ for $k < L$, and $\lambda_{d_k} = 1$ for $k = L$. The final loss function is weighted as $\lambda_{IM} = 1$ and $\lambda_{DFT} = 0.001$.

All scenes are trained for 30,000 steps, with Gaussian refinement enabled in our model for the entire training process. Optimization is performed using SplatFacto’s optimizers, and all experiments are conducted on a single NVIDIA RTX A5000 GPU. For both our model and the baseline SplatFacto model, we incorporate the view-dependent anti-aliased opacity term proposed in Mip-Splatting [19].

4.3. Progressive rendering

Similar to other Level-Of-Detail methods, our method naturally supports progressive rendering, enabling adaptive rendering strategies based on computational resources. On edge devices, such as smartphones and laptops, one can render only the low-frequency Gaussians, either at reduced resolution or at full resolution with lower detail, achieving high frame rates with minimal computational cost. As more powerful GPUs become available, additional high-frequency Gaussians can be rendered to progressively refine the image, as shown in figure 4.

Furthermore, our approach is well-suited for streaming applications, where only the low-frequency Gaussians are to be transmitted first, allowing the end user to start rendering immediately. As demonstrated in Figure 4, transmitting more Gaussians further improves reconstruction quality. See further examples in the supplemental.

Figure 5 compares our approach with that of OCTree-GS [12]. As can be seen, our approach maintains a visually coherent approximation of the scene, as opposed to OCTree-GS.

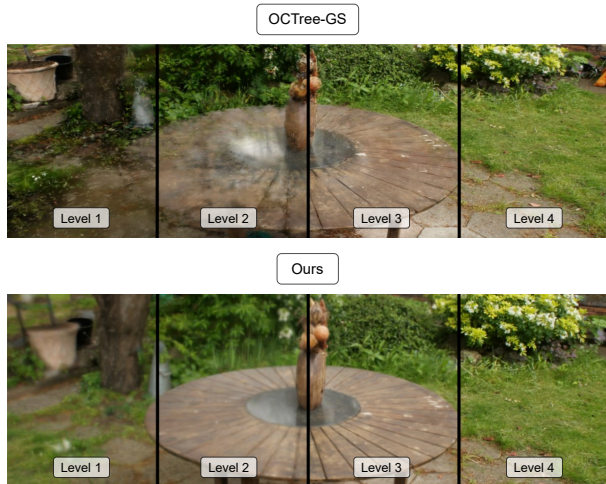


Figure 5. **Progressive Rendering Consistency:** Comparing between OCTree-GS (top) and our method (bottom) across different frequency levels (left to right). In OCTree-GS, lower levels suffer from missing geometric details, which are recovered as more levels are added, leading to artifacts and inconsistent high-frequency details in lower levels. In contrast, our representation preserves the scene’s geometry across all levels, with fine details progressively added, making it more suitable for frequency-aware applications.

4.4. Faster Geometry Interaction

One important application of our frequency decomposition method is fast geometry interaction. Since low-frequency Gaussians define the general structure of the scene, many geometric operations can be efficiently approximated by operating only on this subset. See Figure 5.

We compare the performance of nearest-neighbor search on a randomly sampled 100K point cloud with a scale of 1, using either the full Gaussian set or only the low-frequency subset. Querying the KDTree [2] built from the full model required **1.95 seconds**, whereas querying the KDTree constructed from only the low-frequency Gaussians reduced this to **0.88 seconds**, achieving a $2.21\times$ speedup. Despite this simplification, the median discrepancy was 0.0006, and the mean discrepancy was only 0.0018, corresponding to a 0.18% error relative to the point cloud scale. This result suggests that many geometry-based interactions, such as collision detection and spatial querying, can be significantly accelerated using only the low-frequency representation, with minimal approximation error. The point cloud and the measured scene can be seen in Fig. 6a.

4.5. Foveated Rendering

Our representation enables efficient foveated rendering by dynamically adjusting the contribution of different frequency levels based on eye-tracking input, allowing faster rendering of the region of interest (ROI) relative to the en-

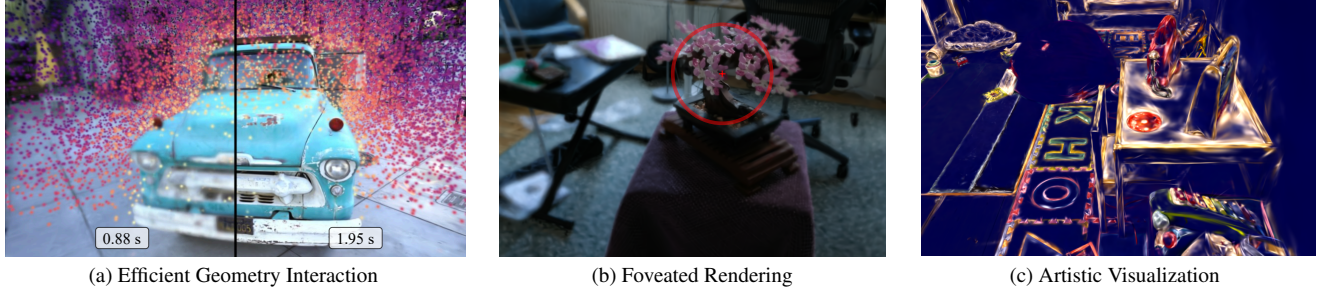


Figure 6. **Applications of Frequency-Based Gaussian Rendering:** (a) Efficient geometry interaction using low-frequency levels for faster processing. Closer points are brighter. Using only low frequency Gaussians (left) is more than twice faster than using all Gaussians (right) with negligible error. (b) Foveated rendering, improving FPS performance using eye-tracking. (c) Frequency-based artistic effects, demonstrating an X-ray-like visualization. Please zoom in for details.

tire image. This is particularly beneficial for AR/VR applications, where optimizing computational resources without sacrificing perceptual quality is critical.

We modulate the contribution of 3D Gaussians at different frequency levels according to gaze-based weighting, discarding those whose effective opacity is below a threshold. As illustrated in Figure 6b, this strategy preserves high-frequency detail in the area where the user is looking while smoothly reducing detail in peripheral regions. Leveraging our multi-resolution representation, we achieve a **40% improvement in FPS** at 4K resolution, significantly reducing rendering costs without sacrificing perceptual fidelity. Further implementation details and additional examples are provided in the supplementary material.

4.6. Artistic 3D Filters

Our representation also enables consistent 3D artistic filtering by selectively modifying the attributes of Gaussians at different frequency levels. By altering specific groups of Gaussians, we can achieve artistic effects that remain coherent across different viewpoints. To demonstrate that, one can use our representation to create X-ray style filter, where low-frequency Gaussians are assigned a constant color of dark blue to simulate an underlying structure, while high-frequency Gaussians have their RGB values increased by 0.2, enhancing the visibility of fine details. As demonstrated in figure 6c, this manipulation creates a 3D-consistent X-ray effect, preserving structural integrity across views. Additional artistic effects on different scenes are showcased in the supplementary material.

4.7. Frequency-Aware 3D Editing

Our method enables 3D-consistent, frequency-aware editing by grouping Gaussians into interpretable frequency subbands. This allows selective edits while preserving scene consistency across multiple views, overcoming the limitations of 2D masks, which can introduce segmentation artifacts and fail to maintain multi-view coherence.

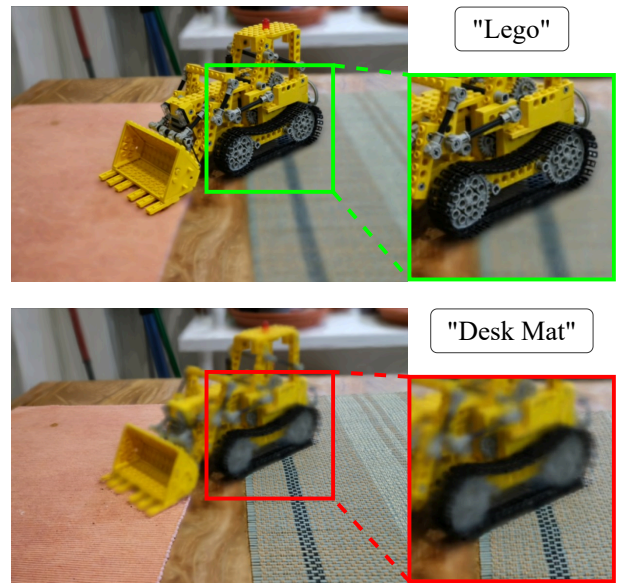


Figure 7. **Frequency Aware 3D Editing:** Our method selectively renders only low-frequency gaussians in the scene, except for gaussians which belongs to the prompted object. The top scene got the prompt "Lego", while the scene at the bottom got "Desk Mat".

We leverage Lang-Segment-Anything [9], which extends SAM2 [11] with text-promptable segmentation. Given a user-defined prompt, SAM2 generates object masks for N randomly selected training images. To identify Gaussians corresponding to the prompted object, we project all Gaussians centers onto each selected image and compute the ratio of occurrences inside a mask relative to successful projections. We preserve Gaussians that either belong to the lowest frequency level or have a mask-projection ratio above a certain threshold, resulting in object-focused rendering where the rest of the scene remains blurred. Importantly, this method not only improves segmentation re-

Dataset	PSNR \uparrow		SSIM \uparrow		LPIPS \downarrow		# Gauss \downarrow	
	Ref	Ours	Ref	Ours	Ref	Ours	Ref	Ours
Mip-NeRF360	29.763	29.651	0.875	0.874	0.146	0.156	824474	789182
Tanks & Temples	24.752	24.399	0.883	0.879	0.102	0.120	480590	493681
Deep Blending	30.288	30.304	0.912	0.914	0.160	0.173	863849	707819

Table 1. Mean reconstruction metrics (PSNR, SSIM, LPIPS) for Mip-NeRF360, Tanks & Temples, and Deep Blending datasets, comparing SplatFacto (Ref) and our model (Ours). The table also includes the average number of Gaussians used in the reconstruction. For this comparison, we rendered all Gaussian levels in our model. All scenes were trained with 3 frequency levels. SplatFacto performs slightly better than our approach. Visually, the differences are barely noticeable.

# Levels	PSNR \uparrow	SSIM \uparrow	LPIPS \downarrow
1 (SplatFacto)	33.683	0.957	0.042
2	33.539	0.957	0.045
3	33.499	0.955	0.049
4	33.289	0.952	0.052

Table 2. Trade-off between the number of frequency groups and reconstruction accuracy. Increasing the number of frequency levels slightly reduces reconstruction accuracy.

liability but also enhances efficiency by rendering fewer Gaussians instead of rendering the entire scene and applying post-processing blurring. Furthermore, this enables the storage of smaller scene representations, allowing emphasis on specific objects without requiring the full dataset.

The entire process runs in seconds to a few minutes, depending on the size of the scene and the number of selected images. Figure 7 illustrates frequency-aware object focus across different text prompts, with additional qualitative results in the supplementary material.

4.8. Ablation Studies

To better understand the contributions of different components in our approach, we conducted a series of ablation studies. These experiments assess the impact of key design choices on model efficiency and rendering quality. All ablation studies were performed on the Kitchen scene from the Mip-NeRF 360 dataset, allowing for consistent evaluation across different configurations. Specifically, we examined (i) *Residual Color Gaussians*, (ii) *Image Loss on Lower Frequency Levels*, and (iii) *Frequency Magnitude Loss*, revealing their respective influences on final rendering quality, memory requirements, and hierarchical decomposition. For a detailed discussion of each ablation, we refer the reader to the supplementary material.

4.9. Limitations

While our method focuses on improving various tasks by leveraging frequency-aware decomposition, it comes with

some slight trade-offs and limitations.

We compare our approach to standard SplatFacto 3D-GS and find there is slight degradation in quality, as can be seen in Table 1. Visually, the differences were hardly noticeable.

Table 2 analyzes the impact of increasing the number of frequency groups on reconstruction accuracy for the "kitchen" scene from the Mip-NeRF360 dataset. As the number of frequency levels increases, PSNR and SSIM exhibit a slight decline, while LPIPS increases. This trend suggests that although higher-frequency decomposition enhances flexibility, it introduces minor degradation in reconstruction quality. Consequently, determining the optimal number of frequency levels requires balancing high-fidelity reconstruction with the benefits of frequency separation.

An additional limitation of our method is the increased training time, which results from the need to regulate multiple frequency levels in both the image and frequency domains. This added complexity leads to longer optimization times compared to the baseline model. However, there is no impact on rendering time or memory consumption during inference, ensuring that our method remains efficient for real-time applications.

5. Conclusions

We introduced frequency decomposition into 3D Gaussian Splatting, inspired by Laplacian pyramids in image processing, to provide structured control over frequency components in a scene. By organizing Gaussians into hierarchical subbands, incorporating Residual Color Gaussians, and leveraging progressive training, our method enhances interpretability and enables efficient level-of-detail management. This approach paves the way for applications such as frequency-aware 3D editing and artistic filtering, allowing precise manipulation of frequency bands for creative effects and content-aware modifications. Furthermore, it supports practical scenarios like foveated rendering, progressive rendering, streaming, and fast geometry interaction, making real-time performance more adaptable across different devices. These capabilities establish our method as a versatile and powerful extension to standard 3D Gaussian Splatting.

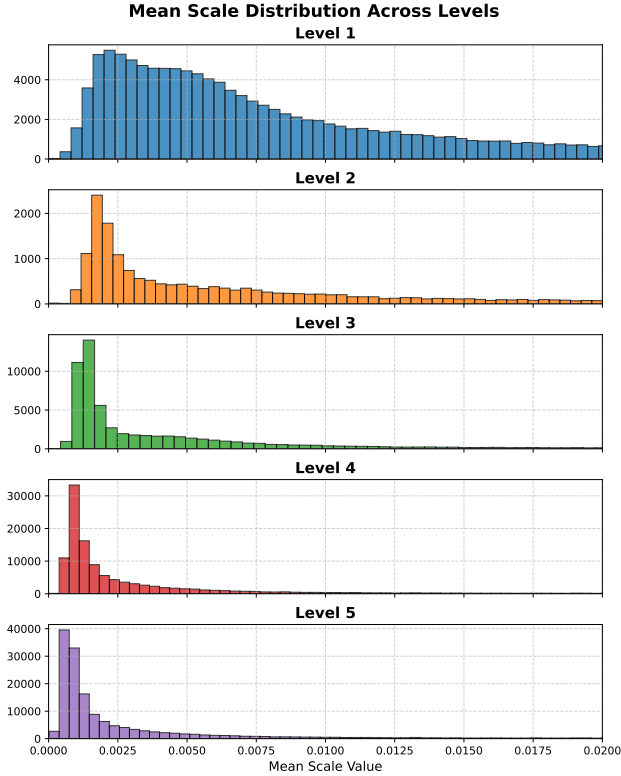


Figure 8. Mean scale distribution of Gaussians across different frequency levels. As the frequency level increases, the distribution shifts toward smaller values, indicating a higher concentration of small Gaussians. This trend highlights the hierarchical nature of the representation, where lower levels capture coarse structures, and higher levels represent finer details.

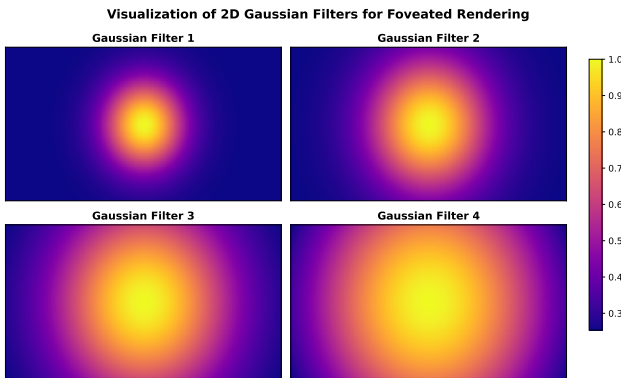


Figure 9. **Gaussian Filtering for Foveated Rendering:** Visualization of the hierarchical 2D Gaussian filters applied to projected 3D Gaussians at different frequency levels. Each filter progressively increases in standard deviation, ensuring that peripheral regions are rendered at lower fidelity while preserving details in the ROI.

6. Supplementary Material

This supplementary document provides additional details, experiments, and qualitative results to complement our main paper. Below is an overview of the contents:

- **6.1 Analysis of Gaussian Scale Distribution Across Levels:** Distribution analysis of Gaussian scales across frequency levels.
- **6.2 Foveated Rendering:** Implementation details of our foveated rendering approach.
- **6.3 Comparison to 3D-GS LOD Methods:** Evaluation of our method against multi-scale 3D Gaussian Splatting baselines.
- **6.4 Efficient Multi-Resolution Rendering with Frequency-Decomposed Gaussians:** Quality analysis of our hierarchical Gaussian decomposition for rendering at low resolutions.
- **6.5 Ablation Studies:** Detailed discussion on key design choices, including residual color Gaussians, frequency magnitude loss, and image loss at lower levels.
- **6.6 Additional Examples of Level of Detail:** Visualization of level-of-detail decomposition in various scenes.
- **6.7 Additional Examples of Foveated Rendering:** Demonstrations of foveated rendering applied to different scenes.
- **6.8 Additional Examples of Frequency-Aware 3D Editing:** Illustration of selective object emphasis using our frequency-aware editing approach in different scenes.
- **6.9 Additional 3D Artistic Filters:** Examples of artistic filters applied to different scenes using our method.

The following sections provide in-depth discussions and results for each of these topics.

The following sections provide in-depth discussions and results for each of these topics.

6.1. Analysis of Gaussian Scale Distribution Across Levels

To gain deeper insights into the characteristics of each frequency level in our representation, we analyze the distribution of the mean scale of the Gaussians, computed as the average of the scale values along the x , y , and z axes for each Gaussian. Figure 8 presents this distribution across different levels.

From the figure, we observe a clear trend: as the frequency level increases, the distribution of mean scales shifts toward smaller values, indicating a higher concentration of small Gaussians. This suggests that higher frequency levels predominantly capture fine details in the scene, represented by numerous small Gaussians, whereas lower frequency levels retain larger-scale structures. The progressive shift in the distribution reinforces the hierarchical nature of our representation, where coarse details are preserved in the lower levels, and finer structures emerge at higher levels.

6.2. Foveated Rendering

To implement foveated rendering, we apply a set of spatially varying 2D Gaussian filters (centered at the fixation point (x, y)) to modulate Gaussians across our frequency levels. Each filter has an appropriately scaled standard deviation to retain peripheral lower-frequency components while prioritizing higher-frequency details in the ROI.

As depicted in Figure 9, these filters serve as soft importance weights for Gaussian opacities. Gaussians with contributions below a predefined threshold are discarded, effectively reducing computational load while maintaining visually coherent, high-detail renderings at fixation. This multi-scale filtering yields a notable 40% FPS improvement at 4K resolution, underscoring its effectiveness for real-time AR/VR applications requiring both efficiency and high visual quality.

6.3. Comparison to 3D-GS LOD Methods

In Table 3, we provide a quantitative comparison of our method against Multi-scale 3D Gaussian Splatting (3DGS) [17], OCTree-GS [12], and SplatFacto [16] in terms of PSNR, SSIM, and LPIPS on Mip-NeRF 360 [1], Tanks & Temples [6] and Deep Blending [4] datasets. Since our approach is implemented in a different framework [15] than Multi-scale 3DGS and OCTree-GS [5], certain implementation details, including downscale resolutions, specific hyperparameter settings and optimization strategies, may not be fully identical. Despite these differences, we include their reported results as a point of reference to provide broader context for our performance evaluation. Our method achieves competitive results to prominent 3D-GS LOD methods, demonstrating its effectiveness in high-fidelity scene reconstruction.

6.4. Efficient Multi-Resolution Rendering with Frequency-decomposed Gaussians

In our method, we use the hierarchical structure of our Gaussian representation to render at lower resolutions efficiently. Specifically, with a 3-level trained model, for $\times 4$ downsampled rendering, we use only the first level of our hierarchy, while for $\times 2$ downscale, we utilize the first two levels. In contrast, the reference method (Splatfacto) directly renders at the target resolution without such hierarchical decomposition. As shown in Table 4, our approach consistently achieves higher PSNR values across different datasets and downscale factors, demonstrating its superior rendering quality at low resolutions. Additionally, since our method processes only a subset of the Gaussians for lower resolutions, it reduces rendering time while maintaining high fidelity.

6.5. Ablation Studies

Effect of Residual Color Gaussians. We evaluated the effectiveness of Residual Color Gaussians by training a model where all Gaussians retained colors in the standard $[0, 1]$ range, rather than using the proposed $[-1, 1]$ residual representation for higher-level Gaussians. This modification led to a significant increase in the total number of Gaussians, from 409K to 515K, representing a 20% growth in scene size. While this increase contributed to a slight improvement in PSNR (+0.2 dB), it also resulted in higher memory consumption and slower rendering times. These findings suggest that the residual color representation enables more compact and efficient scene encoding by allowing individual Gaussians to contribute more effectively to high-frequency details. The ability to add or remove color at different hierarchical levels grants each Gaussian greater expressive power, reducing the overall number of Gaussians required for accurate reconstruction.

Effect of Image Loss on Lower Frequency Levels. To assess the importance of applying the image loss at lower frequency levels, we trained a three-level model while omitting the image loss at lower levels. The resulting model achieved a comparable PSNR to our full method when evaluating the final rendered image; however, its intermediate frequency levels exhibited significant degradation. Specifically, when rendering downsampled resolutions using only the first level (corresponding to a $\times 4$ downsampled output) or the first two levels ($\times 2$ downsampled output), we observed a substantial loss of detail, leading to smeared and blurry reconstructions. Quantitatively, our full model achieved a PSNR of 29.65 dB for $\times 4$ downsampled rendering and 32.27 dB for $\times 2$ downsampled rendering. In contrast, the ablated model, trained without image loss at lower frequency levels, suffered a notable performance drop, with PSNR values of 25.97 dB and 29.36 dB for $\times 4$ and $\times 2$ downsampled renderings, respectively. These results highlight the crucial role of enforcing spatial consistency across frequency levels, ensuring that intermediate levels remain faithful to their expected resolution.

Effect of Frequency Magnitude Loss. We analyzed the impact of the frequency magnitude loss by training the same model without this term. Without frequency regulation, almost all scene details were modeled by the lowest-level Gaussians, while the higher levels contributed almost nothing. This disrupted the intended hierarchical decomposition, as the frequencies were not gradually distributed across levels but instead collapsed into the first level. Consequently, the model failed to leverage the benefits of multi-scale representation, relying predominantly on a single frequency band.

Method	Mip-NeRF360			Tanks & Temples			Deep Blending		
	PSNR \uparrow	SSIM \uparrow	LPIPS \downarrow	PSNR \uparrow	SSIM \uparrow	LPIPS \downarrow	PSNR \uparrow	SSIM \uparrow	LPIPS \downarrow
Multi-scale 3DGS	27.52	-	0.142	23.74	-	0.096	29.70	-	0.096
OCTree-GS	28.05	0.819	0.214	24.68	0.866	0.153	30.49	0.912	0.241
SplatFacto	29.763	0.875	0.146	24.752	0.883	0.102	30.288	0.912	0.160
Ours	29.651	0.874	0.156	24.399	0.879	0.120	30.304	0.914	0.173

Table 3. Comparison of Multi-scale 3D Gaussian Splatting, OCTree-GS, SplatFacto, and Our Method in terms of PSNR, SSIM, and LPIPS. Higher PSNR and SSIM are better, lower LPIPS is better.

Model	MipNeRF-360		Tanks & Temples		Deep Blending	
	x4	x2	x4	x2	x4	x2
Splatfacto	27.739	29.536	23.577	24.819	29.446	30.545
Ours	28.443	29.716	23.812	24.526	29.733	30.597

Table 4. PSNR Comparison between Splatfacto (Reference) and Our Method across different datasets and downscale factors.

6.6. Additional Examples of Level of Detail

In this section, we present qualitative results demonstrating the level of detail captured by our method across various scenes. Figure 10 showcases six different scenarios, each divided into multiple segments, representing different levels of detail in our method’s representation. The images illustrate how our approach captures both coarse structural information and fine details, effectively adapting to the complexity of each scene. The selected examples include objects with varying textures, colors, and geometries, highlighting the versatility of our approach.

6.7. Additional Examples of Foveated Rendering

In this section, we showcase the application of our foveated rendering method across three different scenes: Counter, Playroom, and Train. Each scene contains two renderings for comparison, where the foveation is applied at different regions. The method selectively enhances details in areas of interest while reducing computational load in less critical regions, effectively balancing visual quality and performance. Fig. 11 demonstrates how our approach preserves important details in high-attention areas while applying aggressive downsampling elsewhere.

6.8. Additional Examples of Frequency-Aware 3D Editing

To further demonstrate the effectiveness of our frequency-aware 3D editing approach, we provide additional examples in Figure 12. These results highlight how our method enables selective object emphasis while maintaining 3D consistency. Each row in the figure presents different objects highlighted from a scene using text-based prompts, showcasing the robustness of our 3D voting mechanism. The ap-

proach effectively suppresses background details while preserving high-frequency structures for the selected objects, enabling seamless editing without introducing segmentation artifacts.

6.9. Additional 3D Artistic Filters

We present more examples of artistic filters applied to different scenes using our method, as shown in Figure 13. These effects are achieved by selectively modifying the attributes of Gaussians at different frequency levels.

For the **Brush** effect, we modify the 5-level trained model by keeping level 1 unchanged, while brightening levels 2 and 4 and darkening levels 3 and 5. Additionally, we introduce Gaussian noise to the center positions of Gaussians at levels 2 through 5, resulting in a painterly, textured appearance.

For the **X-ray** effect, we set the colors of Gaussians at levels 1 and 2 to a constant dark shade, simulating an underlying structure. Level 3 is brightened moderately, while levels 4 and 5 are brightened further, enhancing high-frequency details to create a glowing, skeletal appearance.

For the **Sharp** effect, we entirely remove level 2 and set the opacity of levels 3–5 to full, emphasizing fine details. To further enhance contrast, we darken the colors of Gaussians at level 5. This manipulation improves perceived sharpness while maintaining 3D consistency.

References

- [1] Jonathan T Barron, Ben Mildenhall, Dor Verbin, Pratul P Srinivasan, and Peter Hedman. Mip-nerf 360: Unbounded anti-aliased neural radiance fields. In *Proceedings of the IEEE/CVF conference on computer vision and pattern recognition*, pages 5470–5479, 2022. 6, 10

- [2] Jon Louis Bentley. Multidimensional binary search trees used for associative searching. *Communications of the ACM*, 18(9):509–517, 1975. [6](#)
- [3] Peter J Burt and Edward H Adelson. The laplacian pyramid as a compact image code. In *Readings in computer vision*, pages 671–679. Elsevier, 1987. [2](#), [3](#), [4](#), [5](#)
- [4] Peter Hedman, Julien Philip, True Price, Jan-Michael Frahm, George Drettakis, and Gabriel Brostow. Deep blending for free-viewpoint image-based rendering. *ACM Transactions on Graphics (ToG)*, 37(6):1–15, 2018. [6](#), [10](#)
- [5] Bernhard Kerbl, Georgios Kopanas, Thomas Leimkühler, and George Drettakis. 3d gaussian splatting for real-time radiance field rendering. *ACM Trans. Graph.*, 42(4):139–1, 2023. [1](#), [2](#), [3](#), [10](#)
- [6] Arno Knapitsch, Jaesik Park, Qian-Yi Zhou, and Vladlen Koltun. Tanks and temples: Benchmarking large-scale scene reconstruction. *ACM Transactions on Graphics (ToG)*, 36(4):1–13, 2017. [6](#), [10](#)
- [7] Stephane G Mallat. A theory for multiresolution signal decomposition: the wavelet representation. *IEEE transactions on pattern analysis and machine intelligence*, 11(7):674–693, 1989. [2](#)
- [8] Donald Meagher. Geometric modeling using octree encoding. *Computer graphics and image processing*, 19(2):129–147, 1982. [2](#)
- [9] Luca Medeiros et al. Lang-segment-anything: Text-promptable segment anything model, 2023. Accessed: 2025-02-01. [7](#)
- [10] Ben Mildenhall, Pratul P Srinivasan, Matthew Tancik, Jonathan T Barron, Ravi Ramamoorthi, and Ren Ng. Nerf: Representing scenes as neural radiance fields for view synthesis. *Communications of the ACM*, 65(1):99–106, 2021. [1](#), [2](#)
- [11] Nikhila Ravi, Valentin Gabeur, Yuan-Ting Hu, Ronghang Hu, Chaitanya Ryali, Tengyu Ma, Haitham Khedr, Roman Rädle, Chloe Rolland, Laura Gustafson, et al. Sam 2: Segment anything in images and videos. *arXiv preprint arXiv:2408.00714*, 2024. [7](#)
- [12] Kerui Ren, Lihan Jiang, Tao Lu, Mulin Yu, Linning Xu, Zhangkai Ni, and Bo Dai. Octree-gs: Towards consistent real-time rendering with lod-structured 3d gaussians. *arXiv preprint arXiv:2403.17898*, 2024. [2](#), [6](#), [10](#)
- [13] Jonathan Shade, Steven Gortler, Li-wei He, and Richard Szeliski. Layered depth images. In *Proceedings of the 25th annual conference on Computer graphics and interactive techniques*, pages 231–242, 1998. [2](#)
- [14] Claude E Shannon. Communication in the presence of noise. *Proceedings of the IRE*, 37(1):10–21, 1949. [4](#)
- [15] Matthew Tancik, Ethan Weber, Evonne Ng, Ruilong Li, Brent Yi, Terrance Wang, Alexander Kristoffersen, Jake Austin, Kamyar Salahi, Abhik Ahuja, et al. Nerfstudio: A modular framework for neural radiance field development. In *ACM SIGGRAPH 2023 Conference Proceedings*, pages 1–12, 2023. [6](#), [10](#)
- [16] Congrong Xu, Justin Kerr, and Angjoo Kanazawa. Splatfacto-w: A nerfstudio implementation of gaussian splatting for unconstrained photo collections. *arXiv preprint arXiv:2407.12306*, 2024. [10](#)
- [17] Zhiwen Yan, Weng Fei Low, Yu Chen, and Gim Hee Lee. Multi-scale 3d gaussian splatting for anti-aliased rendering. In *Proceedings of the IEEE/CVF Conference on Computer Vision and Pattern Recognition*, pages 20923–20931, 2024. [2](#), [10](#)
- [18] Guandao Yang, Sagie Benaim, Varun Jampani, Kyle Genova, Jonathan Barron, Thomas Funkhouser, Bharath Hariharan, and Serge Belongie. Polynomial neural fields for subband decomposition and manipulation. *Advances in Neural Information Processing Systems*, 35:4401–4415, 2022. [2](#)
- [19] Zehao Yu, Anpei Chen, Binbin Huang, Torsten Sattler, and Andreas Geiger. Mip-splatting: Alias-free 3d gaussian splatting. In *Proceedings of the IEEE/CVF Conference on Computer Vision and Pattern Recognition*, pages 19447–19456, 2024. [6](#)
- [20] Jiahui Zhang, Fangneng Zhan, Muyu Xu, Shijian Lu, and Eric Xing. Fregs: 3d gaussian splatting with progressive frequency regularization. In *Proceedings of the IEEE/CVF Conference on Computer Vision and Pattern Recognition*, pages 21424–21433, 2024. [2](#)
- [21] Junyu Zhu, Hao Zhu, Qi Zhang, Fang Zhu, Zhan Ma, and Xun Cao. Pyramid nerf: Frequency guided fast radiance field optimization. *International Journal of Computer Vision*, 131(10):2649–2664, 2023. [2](#)

Truck



Train



DrJohnson



Counter



Bonsai



Bicycle

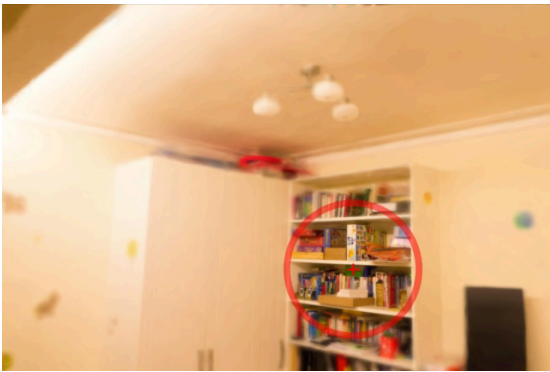


Figure 10. Visualization of the hierarchical detail representation across various scenes using our method. Each image is segmented to illustrate different levels of structural and textural detail captured by our approach. The selected examples—*Truck*, *Train*, *Dr. Johnson*, *Counter*, *Bonsai*, and *Bicycle*—demonstrate its effectiveness across diverse real-world scenarios. Our model is trained with 5 levels, and we render levels 1, 3, and 5 for comparison.

Counter



Playroom



Train



Figure 11. Foveated rendering applied to three different scenes: Counter, Playroom, and Train. Each scene contains two renderings with foveation applied to different areas (highlighted in red). The method prioritizes high-detail rendering in regions of interest while reducing detail elsewhere, optimizing rendering efficiency.

Garden



Counter



Room

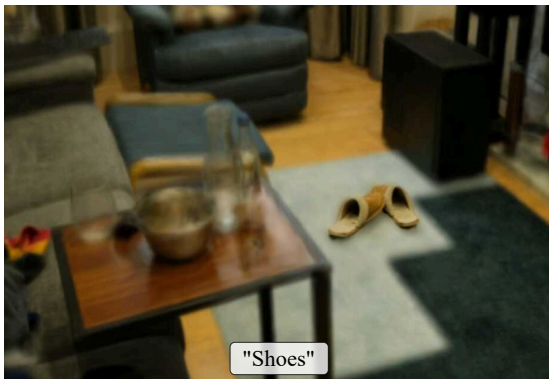
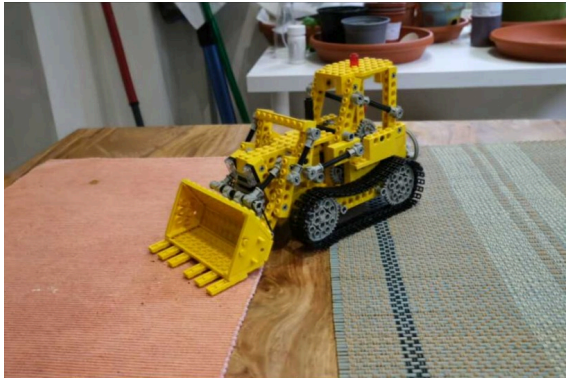


Figure 12. Additional results of frequency-aware 3D editing. Each row shows a different object selected using a text prompt, demonstrating our method's ability to produce consistent 3D object emphasis.

Brush



X-Ray



Sharp



Figure 13. Three artistic effects applied to different scenes using our method. **Top:** The “Brush” effect introduces texture and painterly distortions by adjusting frequency bands and adding positional noise. **Middle:** The “X-ray” effect highlights high-frequency details while suppressing lower levels to create a glowing structural representation. **Bottom:** The “Sharp” effect enhances fine details by removing mid-frequency Gaussians and fully opacifying higher levels.